Second International Conference on Friction Stir Welding, 26-28 June 2000, Gothenburg, Sweden, on cd-rom edited by The Welding Institute TWI, Abington Hall, UK

Effect of Weld Imperfections and Residual Stresses on the Fatigue Crack Propagation in Friction Stir Welded Joints

C. Dalle Donne, G. Biallas*, T. Ghidini and G. Raimbeaux, Institute of Materials Research, German Aerospace Center, D-51170 Cologne Germany

* now with the Department of Materials Science, University of Paderborn, FB 10, D-33095 Paderborn

Abstract

Fatigue crack propagation investigations of defect free and defective friction stir welded joints of 4 mm thick 2024-T3 and 6013-T6 sheets revealed limited effects of the quality of the weld on da/dN-ΔK curves. Residual stress effects are much more important. On the basis of the K_{eff}-approach and a simple residual stress intensity factor estimation it is possible to clear the test data from residual stress effects. The da/dN-ΔK_{eff} curves of the base material and the friction stir welds then fall in a common scatterband, i. e. the fatigue crack propagation properties of base material and FSW joints are very similar.

Introduction

One of the key issues during the material selections for light weight aerospace structures is the fatigue crack propagation (FCP) behavior of long cracks under defined environment. For example, any new material for airplane fuselages in areas where damage tolerance is required, can only be accepted, if the crack growth behavior is not worse than the standard 2024-T3 material [1]. Moreover the "aging aircraft" problem [2] and the trend toward a lager aircraft impel the assessment of the damage tolerance capability of the fuselage structures. This assessment is based on a FCP prediction methodology and the material's resistance to stable fatigue crack propagation expressed by a da/dN-ΔK curve (da/dN is the crack propagation rate and ΔK the applied or nominal stress intensity factor range).

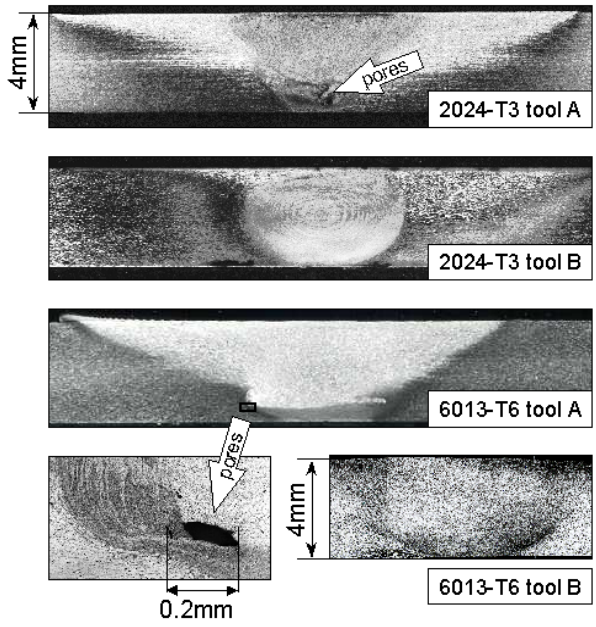

Fig. 1: Cross sections of the friction stir welded joints.

Currently a very limited amount of data on FCP in friction stir welded joints exists [3-5]. Most of the work on fatigue of aluminum friction stir welds (FSW) has been restricted to the generation of S-N data [3, 6, 7]. It was shown in these investigations, that the friction stir welded area in the joints is susceptible to fatigue crack initiation. Especially the notch effects of surface irregularities like the concentric ripples and the overlap weld toe on the advancing side of the weld had a detrimental effect on S-N fatigue life [4, 5, 8, 9]. Skimming of the surface irregularities nullified these notch effects. In the case of joints free of internal defects, the FSW S-N fatigue curves were

comparable to the base material curves [9]. If internal cavities were present, a reduction in fatigue live was observed only in stress ranges above a critical stress level [10, 11]. The critical stress level was estimated by a simple fracture mechanical model requiring the effective (lower bond) base material threshold $\Delta K_{th,eff}$ and a stress intensity factor solution fitting to the size, shape and position of the pores in the weld as input parameters.

Preliminary FCP experiments with welded specimens of the aluminum alloys 2024-T3 [4] and 6013-T6 [5] displayed lower crack growth rates in the weld than in the base material, especially in the range of low crack propagation rates and stress ratios. It has been suggested that increased resistance against FCP is connected to the fine grained material in the weld [3] or to compressive welding stresses in the compact tension specimens used in the FCP investigations [5]. Residual stresses rise (tensile stresses) or lower (compressive stresses) the mean stress or load ratio R of the applied loading. Compared to steel, da/dN-ΔK curves of aluminum alloys are much more sensitive to load ratio effects [12]. Hence, even small amounts of residual stresses (typically attributed to friction stir welds) may have an effect on FCP.

The objective of this paper is to examine the influence of pores and residual stresses on the fatigue crack propagation curves of friction stir welded joints in 2024-T3 and 6013-T6 aluminum alloys.

Materials and Friction Stir Welding

Two types of 4 mm thick aluminum alloy sheets, 2024-T3 and 6013-T6, were welded on conventional milling machines at DLR and DaimlerChrysler on the basis of the TWI procedure described in the patent [13]. The effect of pores on the da/dN-ΔK curves is investigated by comparing friction stir welds produced at the beginning of FSW process development with a very simple tool (tool A) to state-of-the-art joints manufactured more recently with tool B. The main difference between the two tools was that tool B contained a thread whereas tool A did not. Therefore no downward thrust was impelled to the material joined with tool A. If tool B was rotating in the proper direction with respect to its thread, the threads forced down the stirred material and led to a material rotation around the longitudinal axis and the transverse axis of the weld [8, 14]. The rotational flow caused the well known onion ring structure in the cross section of the welds, Fig. 1. In the joints produced with the tool A the downward thrust was absent, hence no onion ring structure is visible. Moreover the lower part of the weld nugget was susceptible to the formation of pores, as shown in Fig. 1 for the 6013-T6 material. In both tool A joints the biggest cavities could be approximated with a 3-dimensional ellipsoid

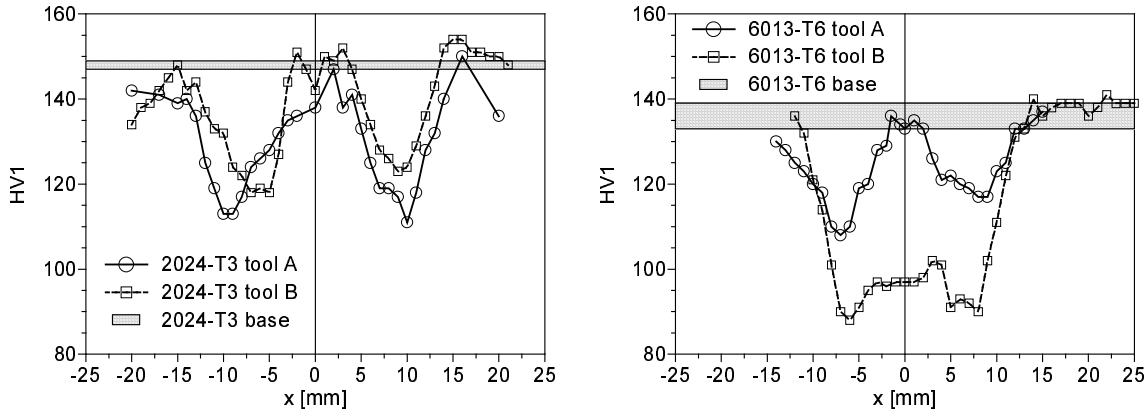

Fig. 2: Hardness profiles taken in the midsection of the FSW joints. x = 0 corresponds to the center of the weld nugget.

having a 0.2 mm long axis perpendicular to the welding direction, a 0.3 mm long axis in welding direction and a 0.07 mm long axis in thickness direction [10]. Several pores were distributed along a string in welding direction. The distance between the borders of two cavities in such a string was at least about 0.3 mm.

The welding direction was always in rolling direction besides for the 2024-T3 tool A joints, which were welded perpendicular to the welding direction. Table 1 summarizes tensile strength values and process parameters of the welds. The hardness distribution in the 2024-T3 joints is consistent with the tensile strength: the tool A joint is characterized by a somewhat lower hardness curve than the tool B, Fig. 2. The differences in hardness and strength in the friction stir welds of 6013-T6 are mainly attributed to the occasion of the T6 aging heat treatment (4h, 190 °C), which was performed after welding in case of the tool A welds and before welding in the case of the tool B welds. The heat treatment after welding probably caused a partial re-precipitation of the β' (Mg_2Si) hardening phases dissolved during the welding process. Therefore the strength and the nugget hardness of the "low quality" (tool A) welds was higher.

Table 1: Static properties of 4 mm thick base materials and FSW joints.

	Orientation	Rotational speed [rpm]	Weld speed [mm/min]	$R_{p0.2}$ [N/mm^2]	R_m [N/mm^2]
2024-T3 base	T			332	478
2024-T3 tool A	L	1000	100	283	395
2024-T3 tool B	T	1000	100	295	425
6013-T6 base	T			349	398
6013-T6 tool A	T	1400	400	292	322
6013-T6 tool B	T	1000	1000	213	305

Experimental Procedure

FCP tests

All fatigue experiments were carried out with constant amplitudes, at room temperature and in laboratory air on a computer controlled servohydraulic testing machine following ASTM E 647 [15]. Crack propagation was monitored through the potential drop technique. In most of the tests, 50 mm wide compact tension specimens (C(T)), Fig. 3, were used for high (R = 0.7 and 0.8) and low (R = 0.1) R-ratio tests. The negative load ratio curves of the 6013-T6 base material and some R = 0.1 curves of welded specimens were obtained from 80 mm wide middle cracked tension specimens (M(T)). All tests with FSW specimens were performed in the "as-welded" condition.

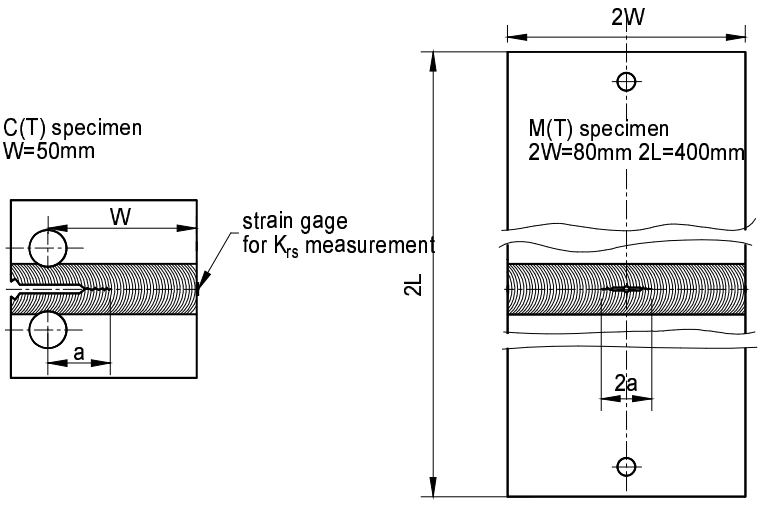

Fig. 3: Specimen for fatigue crack propagation tests.

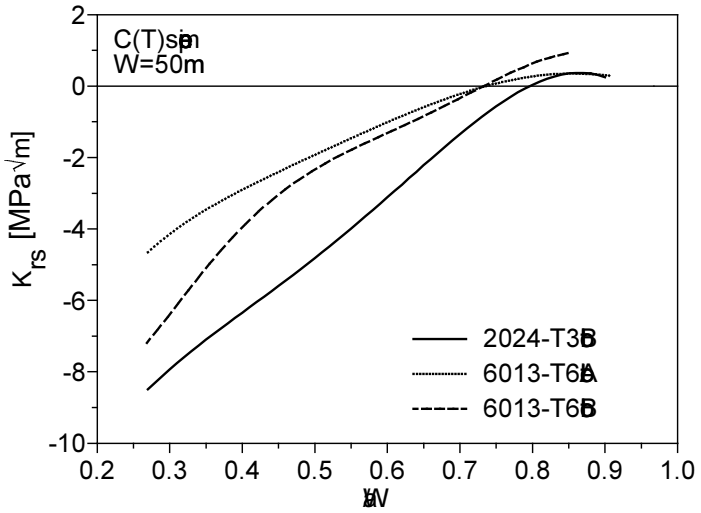

Fig. 4: Distribution of the stress intensity factor due to residual stresses in the ligament of the C(T) specimens.

Residual stress intensity factor measurement

The stress intensity factor due to residual stresses K_{rs} was determined directly with the so called "cut compliance method" [16]. The method is based on the crack compliance method: a narrow saw cut is introduced progressively in the potential crack plane of the considered specimen or component and the resulting strain change is measured by a strain gauge. The desired stress intensity factor is proportional to the slope of the measured strain ε plotted as a function of the depth of the cut (i. e. crack length a):

$$K_{rs} = \frac{E'}{Z(a)} \frac{d\varepsilon}{da} \tag{1}$$

The proportionality factor or influence function Z(a) is a unique function, that depends only on the cut depth, the geometry of the specimen or component and the strain measurement location. For simple geometries Z(a) is obtained by basic relations of linear elastic fracture mechanics.

Besides its simplicity, the great advantage of this method is that it delivers the information about residual stresses in a suitable form for direct use in fracture mechanics. Moreover the elastic re-distribution of residual stresses with increasing crack or slit length is already included in the K_{rs} versus a solution. On the other hand, the determination of the underlying residual stress distribution in the un-cracked structure is not straightforward. If some idea or information about a possible residual stress distribution is available, the exact stress distribution can in principle be obtained with the weight function method [17] by a trail and error procedure. Further information on the verification and accuracy of the cut compliance method may be found in references [18] and [19].

In this investigation a strain gage was glued on the C(T) specimen at the location indicated in Fig. 3. The influence function for the set-up was obtained by a fit of the finite element results of Schindler and Landolt [20]:

$$Z(a) = -\frac{2.532}{(W-a)^{1.5}}\left(1 - e^{-6.694\frac{a}{W}}\right) \quad (2)$$

The crack was simulated by 0.3 mm wide fret saw cuts, which were introduced manually in 1 mm increments. The measured strain versus cut depth (a) data were fitted by third to fifth degree polynomials. These polynomials could be easily differentiated and inserted in eqn. (1).

Fig. 4 shows the distribution of K_{rs} in the ligament of the welded C(T) specimens measured with the compliance cut technique. Mean values of at least 2 cutting test were used for one curve. The joint with the highest yield stress (2024-T3 tool B) is characterized by the highest negative residual stresses. The difference between the two 6013-T6 joints is probably due to the T6 heat treatment: the tool A material was heat treated after welding and a slight relaxation of residual stresses took place during the heat treatment. The negative stress intensity factor curves of Fig. 4 are related to compressive residual stresses ahead of the crack. Apparently the residual stresses re-arrange after a crack growth increment in such way that compressive stresses are maintained at the crack tip. With increasing crack length the magnitude of the compressive residual stresses decreases and finally only small amounts of tensile stresses are active at the tips of long cracks.

Results

Effects of Pores on FCP

The da/dN-ΔK curves of C(T) specimens containing pores (tool A) are compared to defect free joints (tool B) and base materials in Fig. 5. In both materials the deterioration of the FCP properties caused by the pores is much smaller than the drop in fatigue life observed in the S-N tests [4, 10]. Depending on the load level, factors of 3 up to 10 in fatigue life between de-

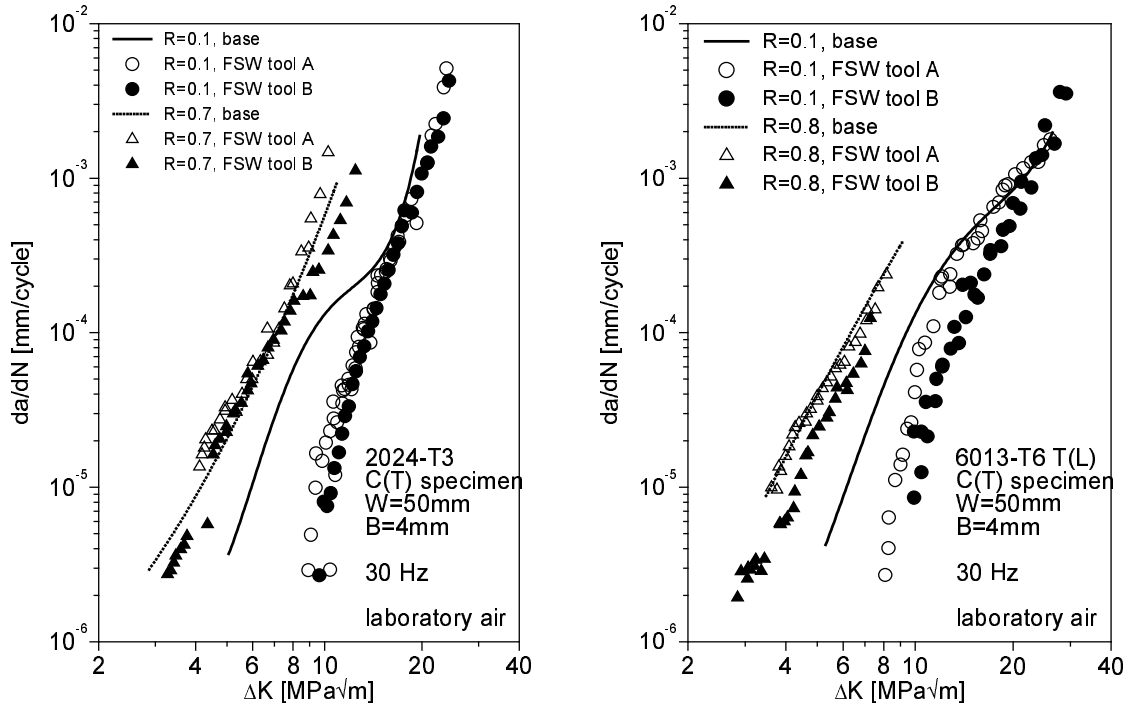

Fig. 5: Fatigue crack propagation curves of joints containing pores (tool A) compared to defect free joints (tool B) and to the base materials.

fect free and defective joints were found in the S-N experiments. It should be recalled here that the 6013-T6 joints were exposed to a slightly different heat treatment procedure. This may be responsible for the higher overall tool A versus tool B discrepancy found in the 6013-T6 joints compared to the 2024-T3 welds.

In both materials an apparent improvement of the FCP properties after friction stir welding is observed at low load and R = 0.1. This effect is attributed to the compressive residual stresses and will be thoroughly discussed in next paragraph. At higher loads and R-ratios, residual stresses were less effective and similar base material and FSW da/dN-ΔK curves were achieved.

It should be noted here, that in the small welded C(T) specimens the plastic zone size validity limit of ASTM E 647 was violated at $\Delta K > 5.4$ MPa√m in the 6013-T6 FSW joints tested at R = 0.8 and at $\Delta K > 8$ MPa√m in the 2024-T3 joints tested at R = 0.7. Since the infraction of the ASTM limits did not alter the general trends of the curves, the complete da/dN-ΔK data sets are presented here.

Effects of Residual Stresses on FCP

Fatigue crack propagation curves of aluminum alloys usually exhibit pronounced R-ratio effects as shown in the left diagram of Fig. 6 for 6013-T6 base material. For a given load ΔK, crack growth rates increase with increasing R. The reason for this behavior is that particularly at low or negative R-ratios only a part of the applied ΔK, designated as the "effective stress intensity factor range ΔK_{eff}", acts as driving force at the crack tip [21]. In other words, ΔK_{eff} is the range between the crack opening stress intensity factor K_{op} at the very crack tip and K_{max} (Fig. 6, center). Irrespective of the applied load ratio, equal ΔK_{eff} values are supposed to result in equal crack propagation rates as shown in the right side of Fig. 6. The underlying physical mechanisms of this effect are still being debated [22]. So far it is important to know, that ΔK_{eff} is usually calculated from empirical relationships which depend on K_{max} or ΔK and R [23]:

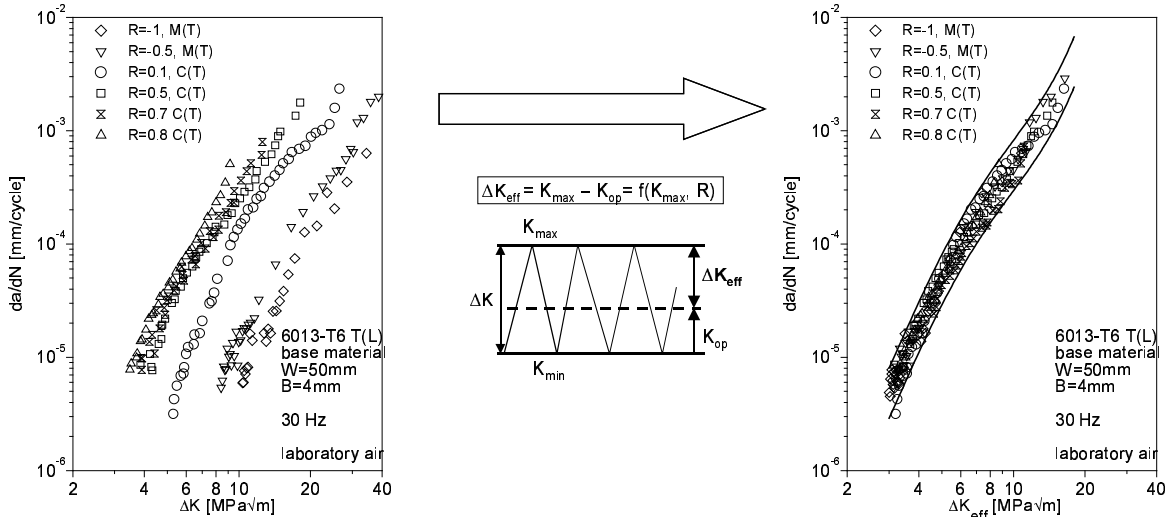

Fig. 6: The effect of R-ratio of on da/dN-ΔK curves (right) is suppressed if the crack propagation rates are plotted as a function of the effective stress intensity factor range ΔK_{eff} (left).

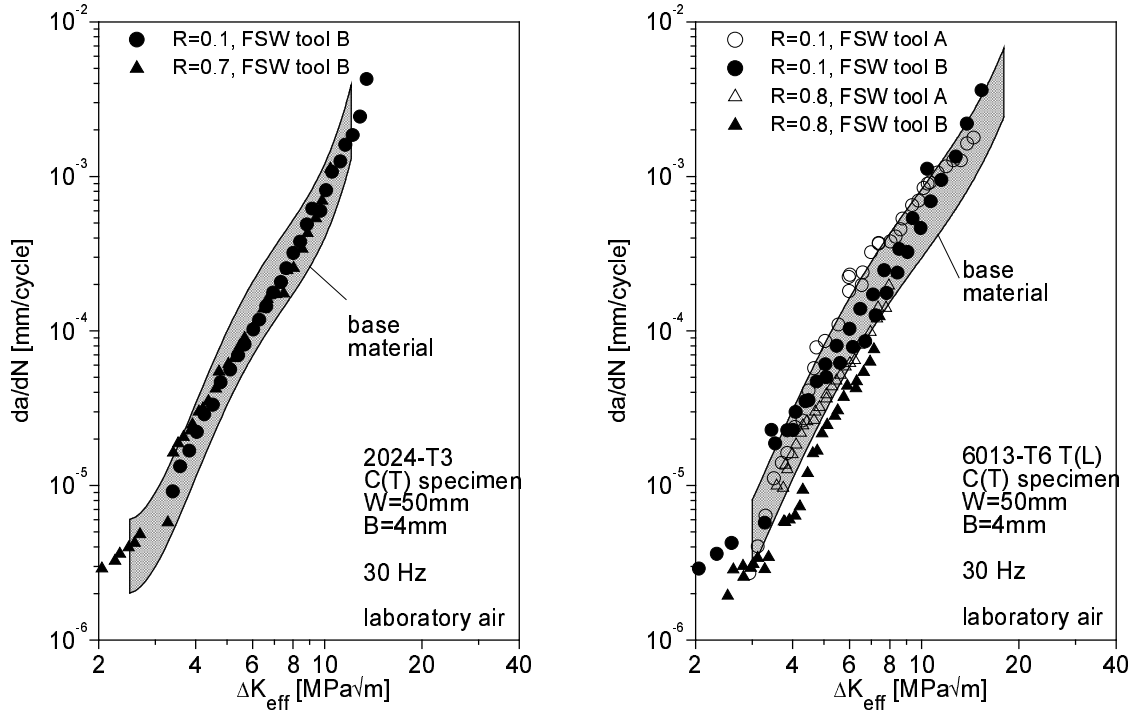

Fig. 7: Effective crack propagation curves of the welded specimens compared to the base material scatterbands.

$$\frac{K_{op}}{K_{max}} = 1 - (1 - R)\frac{\Delta K_{eff}}{\Delta K} = \begin{cases} 1 - (1 - R)(0.55 + 0.33R + 0.12R^2) & \text{for } 2024 - T3 \\ \dfrac{1}{2.097 - 0.811R - 0.297R^2} & \text{for } 6013 - T6 \end{cases} \quad (3)$$

Both solutions are valid in the $-1 \le R \le 1$ range. The 2024-T3 solution was taken from [23]. The 6013-T6 relationship was obtained by shifting the da/dN-ΔK curves on the R = 0.8 curve, where the crack is assumed to be fully open and therefore ΔK equals ΔK_{eff} [24].

When a fatigue crack is propagating in a residual stress field, for example in a welded plate, the stress intensity at the crack front is influenced by the combined effect of residual stresses and the stress resulting from the externally applied (nominal) load. Within the validity limit of linear elasticity the total stress intensity factor acting at the crack tip is given by the sum of the residual stress and external loading contributions (superposition principle) [25-27]. The ΔK value (= $K_{max} - K_{min}$) remains unaffected by K_{rs}, since the residual stress K_{rs} has to be added to the whole nominal or applied loading stress intensity range ΔK. On the other hand the true[1] load ratio R_t is given by:

$$R_t = \frac{K_{min} + K_{rs}}{K_{max} + K_{rs}} \quad (4)$$

It is now possible to calculate the true load ratio on the basis of the K_{rs} versus crack length distributions presented in Fig. 4. Subsequently the effective crack driving force ΔK_{eff} is ob-

[1] The word „effective“ should not be used for this definition of R, since it is usually employed for the description of stress intensities and stress intensity ratios acting locally at the crack tip.

tained under the assumption that equation (3) is applicable also for the friction stir welded microstructures.

If the residual stress contribution is included in the applied load ratio as explained in the previous paragraph, the FCP curves of the welded joints fall in the scatterband of the base materials, Fig. 7. A slight improvement (if any) of FCP behavior after welding is only exhibited by the data of the tool B 6013-T6 friction stir welds, which lie on the right border of the base material scatterband. The ranking of the 6013-T6 tool A versus tool B welds observed in Fig. 5 is retained when the crack propagation rates are plotted as a function of K_{eff} in Fig. 7. Since residual stress effects are sorted out, a small degradation of FCP properties due to pores (and/or heat treatment) can be granted to this material. More important is the fact that the apparent improvement of FGP properties at low loads and load ratios displayed in Fig. 5 is solely caused by compressive residual stresses present in the crack tip region of the C(T) specimens.

The question arises now, if crack propagation curves measured with another specimen geometry and therefore a different residual stress distribution yield also different nominal da/dN-ΔK curves. In Fig. 8 R = 0.1 FCP curves of center cracked M(T) specimens are compared to the curves measured with edge cracked C(T) specimens. Indeed large discrepancies are found in the case of the welded specimens, whereas the base material curves lie in a common scatterband as expected. Evidently the machining of the specimens and the crack starter notches generated different re-arrangements of residual stresses in C(T) and M(T) specimens.

Fig. 9 shows schematic trends of the residual stresses perpendicular to the weld in a welded plate and in C(T) and M(T) specimens machined from a welded plate with such a stress distribution. Otha et al. [28] investigated these stress distributions in gas metal arc welded steel joints by X-ray measurements. In welding, residual stresses are generally a result of the impediment of shrinkage of the hotter weld zones by the surrounding cooler zones [29]. A simi-

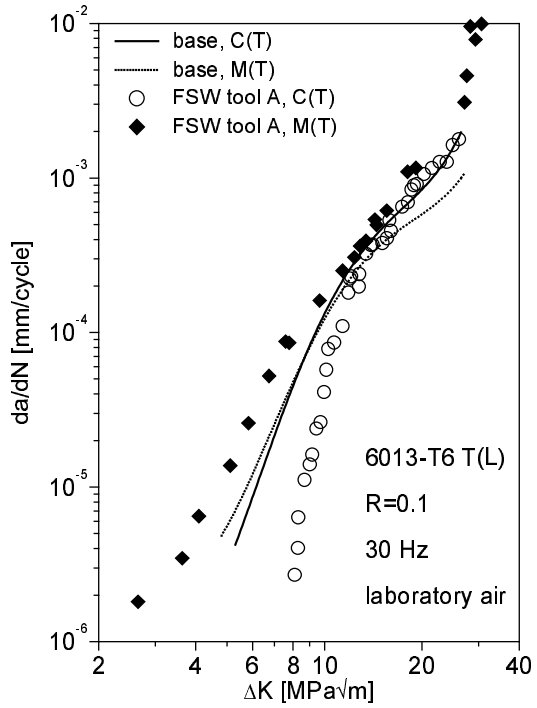

Fig. 8: Influence of specimen geometry on nominal da/dN-ΔK curves.

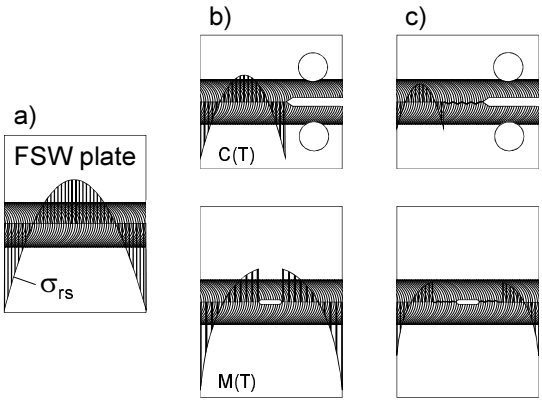

Fig. 9: Schematic of residual stress distribution in a friction stir welded plate a), stress redistribution after machining of specimens b) and during crack growth c) [28].

lar stress distribution is supposed to be present also in friction stir welded plates. After machining of the specimens, compressive residual stresses were present at the crack tip of a C(T) specimen whereas tensile stresses were active at the crack tip of M(T)-specimen. As discussed in connection with Fig. 4, the crack tip stresses remained compressive (C(T)) or tensile (M(T)) also during subsequent crack growth. Considering R-ratio dependence of the base material data of Fig. 6, higher crack velocities than in C(T) specimens were expected and actually obtained with M(T) specimens loaded at the same nominal ΔK.

Concluding Remarks

Fatigue crack propagation investigations of defect free and defective friction stir welded joints of 4 mm thick 2024-T3 and 6013-T6 sheets revealed limited effects of the quality of the weld on da/dN-ΔK curves. Residual stress effects are much more important. Ignoring residual stress effects may lead to unconservative estimations of the FCP behavior of friction stir welds, especially if edge cracked specimens are used and low R-ratios are applied. Moreover, crack propagation curves will depend on specimen geometry and size, since the distribution of residual stresses is geometry dependent.

On the basis of the K_{eff}-approach and a simple residual stress intensity factor estimation it is possible to eliminate the residual stress effects from the test data. The da/dN-ΔK_{eff} curves of the base material and the friction stir welds then fall in a common scatterband, i. e. the FCP properties of base material and FSW joints are very similar.

In process parameter optimization investigations or in the case of comparison between welds of different materials it is always suggested to perform some tests at high load ratios ($R > 0.5$), regardless of the utilized specimen type or size. At high load ratios aluminum alloys are generally less sensitive to load ratio effects. Therefore residual stresses have a very limited effect on FCP and meaningful material data is measured.

Acknowledgements

The authors wish to thank Mrs. C. Juricic, Mr. U. Fuchs, and Mr. H.-W. Sauer for their support in welding and in the experimental investigations and Mr. F. Palm from DaimlerChrysler, Munich, for kindly providing some of the FSW joints.

References

[1] Schmidt-Brandecker B. and Schmidt, H.-J.: NATO Research and Technology Organization's Workshop 2 on Fatigue in the Presence of Corrosion,1998.

[2] Schijve, J.: Fatigue Fract. Engn. Mater. Struct., 18, 3, 1995, pp. 329-344.

[3] Haagensen, P.J., Midling, O.T. and Ranes, M.: 2nd International Conference on Surface Treatment 95, Vol. II, 1995, pp. 225-237.

[4] Dalle Donne, C. and Biallas, G.: European Conf. on Spacecraft Structures, Materials and Mechanical Testing, Stavrinidis, C., Rolfo, A. and Breitbach, E. (Eds.), ESA SP-428, 1999, pp. 309-314.

[5] Braun, R., Biallas, G., Dalle Donne, C. and Staniek, G.: Materials for Transportation Technology EUROMAT '99 - Vol. 1, Winkler, P.J. (Ed.), Wiley-VCH, 1999, pp. 150-155.

[6] Ranes, M., Kluken, A.O. and Midling, O.T.: Trends in Welding Research, Proceedings of the 4th International Conference, ASM, 1995, pp. 639-644.

[7] Hori, H., Makita, S. and Hino, H.: 1st International Symposium on Friction Stir Welding, TWI, UK, 1999, pdf-file.
[8] Biallas, G., Braun, G., Dalle Donne, C., Staniek, G. and Kaysser, W.: ibid.
[9] Bussu, G. and Irving, P. E.: ibid.
[10] Biallas, G., Dalle Donne, C. and Braun, R.: 32. Tagung des DVM-Arbeitskreises Bruchvorgänge, DVM-Bericht 232, DVM, Berlin, 2000, pp. 203-212.
[11] Biallas, G., Dalle Donne, C. and Juricic, C.: to be presented at EUROMAT 2000, Tours, France 7-9 November 2000.
[12] Bucci, R.J.: ASM Handbook Vol. 19, Fatigue and Fracture, Lampman, S.R. (Ed.), ASM International, 1996, pp. 771-812.
[13]Thomas, W.M., Nicholas, E.D., Needham, J.C., Murch, M.G., Templesmith, P. and Dawes, C.J.: Improvements Relating to Friction Welding, European Patent, EP 0 615 480 B1, 1992.
[14] Staniek, G., Hillger, W. and Kurze, P.: DVS, BDLI Sondertagung: Moderne Werkstoffe im Luft- und Raumfahrzeugbau, DVS, 2000, to be published.
[15] Bachmann, V., Marci, G. and Sengebusch, P.: Automation in Fatigue and Fracture: Testing and Analysis, ASTM STP 1231, Amzallag, G. (Ed.), ASTM, Philadelphia, 1994, pp. 146-163.
[16] Schindler, H.-J., Cheng, W. and Finnie, I.: Experimental Mechanics, 37, 3, 1997, pp. 272-277.
[17] Parker, A.P.: Residual Stress Effects in Fatigue, ASTM STP 776, ASTM, 1982, pp. 13-31.
[18] Schindler, H.-J.: 5th European Conference on Residual Stresses,1999, in press.
[19] Prime, M.B.: Fatigue Fract. Engn. Mater. Struct., 22, 1999, pp. 195-204.
[20] Schindler, H.-J. and Landolt, R.: Proc. of the 4th European Conf. on Residual Stresses,1996, pp. 509-517.
[21] Elber, W.: Engng. Fracture Mech., 2, 1970, pp. 37-45.
[22] Lang, M. and Marci, G.: Fatigue and Fracture Mechanics: 29th Volume, ASTM STP 1321, Panontin, L. and Sheppard, D.S. (Eds.), ASTM, 1999.
[23] Schijve, J.: Mechanics of Fatigue Crack Closure, ASTM STP 982, Newman, J.C and Elber, W (Eds.), ASTM, Philadelphia, 1988, pp. 5-34.
[24] Zhang, C., Marissen, R., Schulte, K., Trautmann, K.-H., Nowack, H. and Schijve, J.: Fatigue Fract. Engn. Mater. Struct., 10, 4, 1987, pp. 315-332.
[25] Elber, W.: Fracture Toughness and Slow Stable Cracking, ASTM STP 569, ASTM, 1974, pp. 45-58.
[26] Glinka, G.: Fracture Mechanics, ASTM STP 677, Smith, C.W. (Ed.), ASTM, 1979, pp. 198-214.
[27] Beghini, M. and Bertini, L.: Engng. Fracture Mech., 36, 3, 1994, pp. 379-387.
[28] Ohta, A., Sasaki, E., Nihei, M., Kosuge, M. and Inagaki, M.: Int. J. Fatigue, 4, 1982, pp. 233-237.
[29] Masubuchi, K.: Analysis of Welded Structures, Pergamon Press, 1980.